Turnitin_Lidya10

by Lidya Anggraeni

Submission date: 07-May-2026 11:19AM (UTC+0700)
Submission ID: 2954779727
File name: Modeling_of_Magnetorheological_Damper.pdf (975.28K)
Word count: 5867
Character count: 29598

MODELING OF MAGNETORHEOLOGICAL DAMPER USING MULTIPLE ARTIFICIAL NEURAL NETWORKS FOR FUZZY CONTROL DESIGN OF A SEMI-ACTIVE SUSPENSION SYSTEM

Erwin SITOMPUL[1], Lydia ANGGRAINI[2], Arjon TURNIP[3]

Suspension is a very important part of the functionality of a car. It supports the comfort of the passengers and can be used to improve the car's stability. If a magnetorheological (MR) damper is used, the damping performance can be adjusted according to the road condition. In this research, an attempt to model an MR damper using multiple artificial neural networks (ANNs) was conducted. The measurement data was obtained by using a damper dynamometer. Eight measurements were conducted to cover the coil current range between 0 and 1,400 mA. The MR damper model was then integrated into the semi-active suspension of a quarter-car model. Furthermore, the fuzzy logic controller (FLC) design for the semi-active suspension system was conducted. This artificial intelligence control deployed a novel approach in using the frequency content of the road surface as the input. The control scheme was tested by giving a sinusoidal bumpy road and a pseudo-random bumpy road as the input to the quarter-car model. The FLC performed well and was able to reduce the transmitted excitation from the road to the car chassis.

Keywords: magnetorheological (MR) damper, semi-active suspension, artificial neural networks (ANN), fuzzy logic controller (FLC)

1. Introduction

The development of automotive technology also increases the safety and comfort standards demanded by car users as well as environmental considerations [1-2]. One factor that can be the source of discomfort is oscillation due to the uneven road surface transmitted by the suspension system to the car chassis and experienced by passengers.

A good suspension system provides a trade-off between stiffness and softness while withstanding the shocks caused by the road surface that contains

[1] Assoc. Prof., Study Program of Electrical Engineering, President University, Cikarang, Indonesia, e-mail: sitompul@president.ac.id
[2] Assoc. Prof., Study Program of Mechanical Engineering, President University, Cikarang, Indonesia, e-mail: lydia.anggra@president.ac.id
[3] Assoc. Prof., Department of Electrical Engineering, Padjajaran University, Bandung, Indonesia, e-mail: turnip@unpad.ac.id

low and high-frequency contents [3]. Thus, an adaptive suspension system is required to minimize oscillation transmission and its effects, where the system is expected to adjust the damping force based on varying road surfaces. This adaptivity and adjustability based on measured vehicle ride and handling indicators can be provided by a semi-active suspension system.

In a semi-active suspension system, the flow of the damper fluid can be regulated by using various valve mechanisms, such as electromechanical or electromagnetic valves. In an electromagnetic valve, the flow of the fluid is influenced by an electromagnetic field that affects the viscosity of the fluid [4-6]. Such a fluid whose viscosity can be varied depending on the applied electromagnetic field is called magnetorheological (MR) fluid, which is composed of ferromagnetic particles in the order of micrometers besides carrier fluids and some additives [1,7]. The damper with MR fluid has a certain characteristic relation of damping force versus piston velocity for a given electric current fed to its electromagnetic circuit [8-10].

In this paper, the modeling of an MR damper and its utilization in designing an artificial-intelligent control scheme of a semi-active suspension system will be presented. A novel model structure for the damping-force to piston-velocity relation of the MR damper was devised using multiple artificial neural networks (ANN) and linear interpolation [8,11]. A pre-defined electric current was fed to the MR damper, and a dedicated ANN modeled its effect on the damping performance.

Afterward, the MR damper model was integrated into a semi-active suspension of a quarter-car model, consisting of one tire as unsprung mass, one car chassis as sprung mass, two springs, and the MR damper. Then, a unique artificial-intelligent-based control was developed to optimally regulate the semi-active suspension model when the quarter-car model was introduced to varying road surface conditions, such as a simulative speed bump, bumpy road, and pseudo-random bumpy road [12-14]. Thus, optimized driving comfort can be achieved for various road conditions [15].

2. Modeling of MR Damper

2.1. Basic Theory of MR Damper

In a car suspension system, the function of a damper is to dissipate the excitation energy received by the tire from the road and thus reduce the oscillation and vibration transmitted to the car chassis. The reaction force produced by a damper comes from the energy required to flow the fluid through the orifice as the piston moves with a certain velocity.

In its simplest mathematical modeling, the damping force is taken as a multiplication between the damper coefficient b and the piston velocity. However,

in reality, this relation is nonlinear, with *b* having a greater value in the lower velocity and a smaller value in the higher velocity.

Conventional dampers only have a single function to relate the damping force and the piston velocity. On the other hand, an MR damper has an additional free variable, which is the current flowing to the electromagnetic coil. Fig. 1(a) shows the functional diagram of an MR damper. It has coils that if given an electric current, will generate an adequate electromagnetic field to influence the orientation of the MR fluid particles, increase the overall fluid viscosity, and finally increase the damping coefficient [16].

The damping-force to piston-velocity relation of an MR damper can be seen in Fig. 1(b). The shaded area shows the region where the MR damper can operate within the range of the input current. For a given piston velocity, the greater the current is given to the damper, the higher the resulting damping force will be [17].

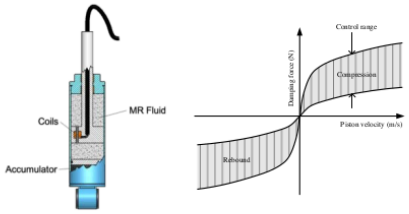

(a) (b)

Fig. 1. (a) The sketch of the MR damper [18]; (b) The working range of an MR damper

Fig. 2(a) shows the MR damper investigated in this research. The damper of type C45-55B01 was manufactured by Bohai New Materials Co., Ltd. It was designed for low voltage and low energy consumption. The damping coefficient can respond to the change in magnetic field change in less than 15 ms. The maximum allowed electric current feed is 1.5 A. The dimension of the MR damper is depicted in Fig. 2(b), while some basic information is summarized in Table 1.

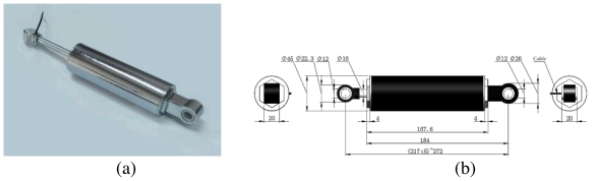

(a) (b)

Fig. 2. Magnetorheological (MR) damper Bohai C45-55B01
(a) The image; (b) The technical drawing [18]

Table 1

Parameters of the MR damper [18]

Item	Value
Stroke	55 ± 5 mm
Damping force	270-2250 N/(m/s)± 10% at 100 mm/s
Current	0-1.5 A
Resistance	5 Ω
Pressure of accumulator	2 MPa

2.2. Artificial Neural Network (ANN)

Artificial neural networks resemble human biological neural networks through the interconnections of neurons and weights. The neuron model utilized in this paper is shown in Fig. 3.

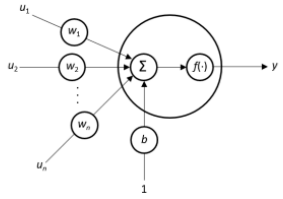

Fig. 3. The neuron model

The inputs of a neuron (u_i) are multiplied with the corresponding weights (w_i) first, and the summation is given as the input of an activation function $f(.)$. The following equations govern the calculation of the neuron output.

$$net = \sum_{i=1}^{n} w_i u_i + b \tag{1}$$

$$y = f(net) \tag{2}$$

As a continuous differentiable function, the tangent sigmoid is chosen to be the activation function of the ANN. An ANN with a single hidden layer is considered a universal approximator that can approximate any continuous function with a certain accuracy if its parameters, *i.e.*, weights and biases, are properly assigned. A learning phase is conducted to find the best parameter set θ for the ANN to minimize the cost function E,

$$E(\boldsymbol{\theta}) = \frac{1}{2} \sum_{j=1}^{m} (y_{\mathrm{m}}(\boldsymbol{\theta}) - y)^2 \tag{3}$$

where y_{m} is the ANN output and y is the expected output.

The backpropagation learning method applies the negative gradient optimization method, which updates the parameters to the direction opposite to the gradient of the cost function E with respect to the parameters,

$$\boldsymbol{m}_{\text{new}} = \boldsymbol{m}_{\text{old}} - \eta \boldsymbol{G} \tag{4}$$

where η is the learning rate variable and $\boldsymbol{G} = \partial E / \partial \boldsymbol{\theta}$.

2.3. Proposed Modeling Approach

It was apriori known that the input current range of the MR damper was between 0 and 1.5 A, and the velocity range of the piston velocity varied between −0.4 m/s and +0.4 m/s during the experiment. This control range, as shown in Fig. 1(b), was to be covered by a number of ANNs responsible for the whole piston velocity range but only for pre-defined current values. For other current values than the pre-defined ones, an interpolation method was used to find the best estimate of the damping force produced by the MR damper.

The structure of the ANN chosen to model the MR damper is shown in Fig. 4. The network has one hidden layer with four neurons. The activation function for the neurons in the hidden layer is tangent sigmoid, while for the output neuron, it is linear.

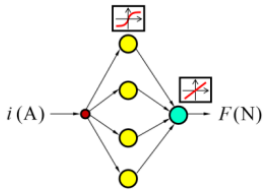

Fig. 4. The ANN to model the MR damper

The interpolation between the curves of two pre-defined current values is shown in Fig. 5. If the ANN model for a certain current is not available, as shown by the red dot, then the damping force must be interpolated by using the values from the two closest ANN models, the blue and the green dots. The interpolation calculation is given by

$$F_{v_a,i} = F_{v_a,i_1} + \frac{i - i_1}{i_2 - i_1}\left(F_{v_a,i_2} - F_{v_a,i_1}\right) \tag{5}$$

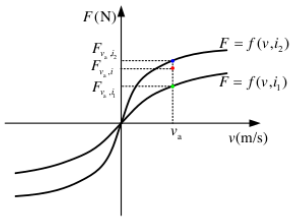

Fig. 5. The interpolation to obtain the damping force for given piston velocity v_a and coil current i.

3. Control of Semi-Active Suspension Using Fuzzy Logic Controller

3.1. Quarter-Car Model

A quarter-car model is the simplest representation of a vehicle in dynamic analysis. Fig. 6 shows the diagram of a quarter-car model. It describes the essential movements of the vehicle parts, namely the sprung mass (car chassis, m_2) and the unsprung mass (tire, m1), all in the vertical translational direction. The tire is assumed to be visco-elastic with a constant stiffness (k_w). The car chassis is rigidly connected to the tire through a damper (b) and a spring (k_s).

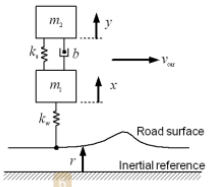

Fig. 6. The quarter-car model

The input to the model is the road surface (r), which results in the displacement of the tire (x), the displacement of the car chassis (y), the vertical velocity of the tire, and the vertical velocity of the car chassis

The ordinary differential equation that expresses the quarter-car suspension model can be given by two ordinary differential equations as follows:

$$\ddot{x}+\frac{b}{m_1}(\dot{x}-\dot{y})+\frac{k_s}{m_1}(x-y)+\frac{k_w}{m_1}x=\frac{k_w}{m_1}r \tag{6}$$

$$\ddot{y}+\frac{b}{m_2}(\dot{y}-\dot{x})+\frac{k_s}{m_2}(y-x)=0 \tag{7}$$

In this research, the parameters of the quarter-car model were chosen to match the specifications of a small city car. In Indonesia, this car was aimed to be the class of Daihatsu Ayla. This consideration was based on the future plan to implement the research result in such a car class in real life. These parameters are compiled in Table 2.

The sprung mass was based on the car's weight of 850 kg without passengers. The mass of the tire and the rim was approximated to be 40 kg. The damping coefficient of 2750 N/(m/s) was based on the data obtained from a standard damper's test of a Daihatsu Ayla. The tire stiffness and chassis stiffness were the values taken within the value range as reported by several sources [19-21].

Table 2

Parameters of the quarter-car model

Parameter	Term	Value	Unit
m_2	Sprung mass	250	kg
m_1	Unsprung mass	40	kg
k_s	Car chassis stiffness	55,000	N/m
b	Damping coefficient	3,500	Ns/m
k_w	Tire stiffness	265,000	N/m

3.2. Proposed Control Scheme

A fuzzy logic controller (FLC) is a control approach that integrates the human way of thinking. It is a normal daily matter to decide based on certain conditional statements in the form of "IF … THEN …" rules. Fuzzy control uses a set of these rules to relate the input variables of the controller to the output variables. For further improvements, the rules can also be optimized by using various optimization methods such as those applied in [22] and [23]

Fig. 7 shows the diagram of an FLC where its core is the rule base (set of rules) and the inference engine. This engine is used to determine the contribution of each rule to the output.

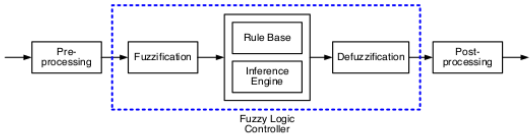

Fig. 7. The block diagram of the fuzzy logic controller (FLC)

Any real measurement value can be pre-processed to adjust the variable range before being given to the fuzzification process. Here, the crisp value is converted into membership value with the logic values of [0,1]. Only firing rules will contribute to the output. After the aggregation of the firing rules' contribution, a

crisp value must again be determined as the output of the FLC. If required, this value can be post-processed to suit the variable range.

The proposed control scheme to realize the artificial intelligence control of the semi-active suspension system using an MR damper is presented in Fig. 8. Road surface excitation is given as the input of the suspension system. The outputs of the system are used by the MR damper (piston velocity) [24].

The FLC transmits the optimal current as the output to the MR damper. Thus, it is crucial to design a rule base that covers all eventualities of the operation. Through the adaptable damping coefficient values, it is expected that the performance of the suspension system can be improved and the control objective in the form of the set point can be better achieved.

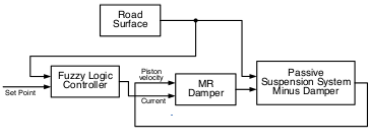

Fig. 8. The control scheme of the MR damper for semi-active controller

4. Results and Discussion

4.1. Characteristics of MR Damper

The measurement of the MR damper characteristics was conducted by using a damper dynamometer or shock dyno, as seen in Fig. 9.

Fig. 9. Experimental setup using damper dynamometer

The upper mount and the lower mount of the damper were first fixed to the dynamometer. Afterward, a crankshaft rotated and gave a certain up-and-down velocity to the piston. During one experiment, the piston speed was varied from 0 to 0.40 m/s with an interval of 0.05 m/s. The piston velocity during a compression (the piston pressing into the damper) was taken as positive, while during a rebound (the piston releasing out to the normal position) was taken as negative.

Since the input electric current to the MR damper can be up to 1.5 A, the experiment was repeated for eight different currents with an interval of 200 mA, starting from 0 to 1,400 mA. At the end of the last experiment, eight measurement results were obtained. Their representation in the damping-force to piston-velocity graph is shown in Fig. 10.

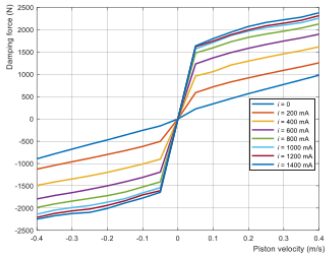

Fig. 10. The measurement results of the damper dynamometer

4.2. Model of MR Damper

The modeling result of the MR damper using ANN is shown in Fig. 11.

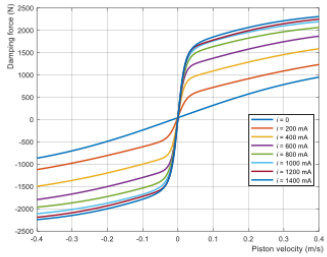

Fig. 11. The output of ANNs for all pre-defined current values

The critical merit of the application of the ANN model here is for the velocity value between 0 and ±0.05 m/s, where a direct linear line clearly cannot represent reality. The seamless quasi-exponential increase of the damping force at the low velocity is preferred. The smooth transition between graphs with increasing current values is outstanding. The distance between two neighboring graphs is also coherent across the considered velocity range.

4.3. Test of MR Damper Model

The model of the MR damper was realized in Matlab Simulink for further simulation purposes. The result is shown in Fig. 12. The piston velocity was fed to all ANNs from the first input. However, only the corresponding interpolated value was passed as the output, depending on the value of the current to the coil, *i.e.*, the second input.

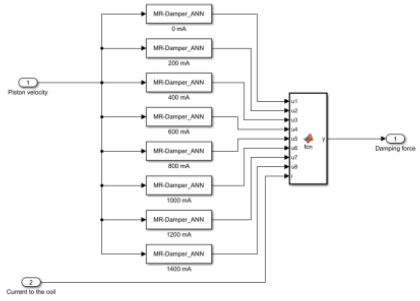

Fig. 12. The model of the MR damper using multiple ANNs

The obtained MR damper model was then put to the test. The piston velocity was varied from −0.40 m/s to +0.40 m/s, as shown by the top graph in Fig. 13. At the same time, the current was varied following a sinusoidal function with a bias of 600 mA and an amplitude of 300 mA. This means that the current to the coil was varied between 300 mA and 900 mA. This is shown in the middle graph in Fig. 13.

Thus, five ANNs are included in the damping force calculation, representing the currents 200 mA, 400 mA, 600 mA, 800 mA, and 1,000 mA. The bottom graph in Fig. 13 shows the outputs of the five ANN models (thin lines) and the interpolation results (thick blue line). The thick blue line wandered up and down, claiming the values between the 200 mA line and the 1,000 mA line, according to the value of the current to the coil.

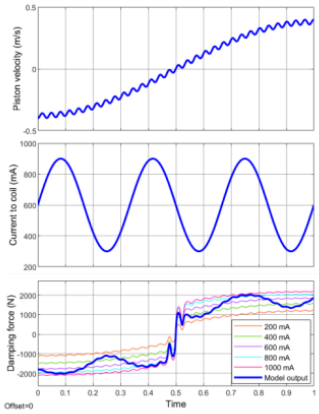

Fig. 13. The test of MR damper model

This test confirmed the functionality of the MR damper model using multiple ANNs.

4.4. Analysis of Quarter-Car Model

The realization of the passive suspension system, as described by Eqs. 6 and 7, is presented in Fig. 14. The green triangle depicts the constant damping coefficient b, which will later be a variable in modeling the semi-active suspension system.

The time response and the frequency response of the quarter-car system were first investigated to find the effect of the damping coefficient b on the system output. The transfer function of the quarter-car model can be derived into the transfer function form presented in Eq. 8.

$$\frac{Y(s)}{R(s)} = \frac{\dfrac{k_w b}{m_1 m_2}\left(s + \dfrac{k_s}{b}\right)}{s^4 + \left(\dfrac{b}{m_1} + \dfrac{b}{m_2}\right)s^3 + \left(\dfrac{k_s}{m_1} + \dfrac{k_s}{m_2} + \dfrac{k_w}{m_1}\right)s^2 + \left(\dfrac{k_w b}{m_1 m_2}\right)s + \dfrac{k_w k_s}{m_1 m_2}} \tag{8}$$

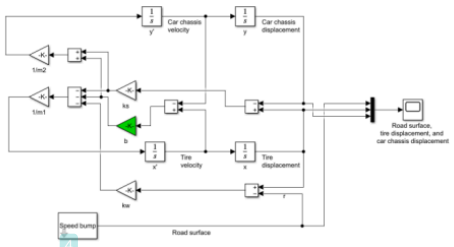

Fig. 14. The model of a quarter-car model with a passive damper in Matlab Simulink

The unit step response of the quarter-car model for various damping coefficients is shown in Fig. 15(a). For an input with low-frequency content, such as a step function, the rise time, the peak time, and the settling time decrease as the damping coefficient increases.

Fig. 15(a) also shows that the quarter-car model is a stable system. The change of b will not affect the system's stability. Nevertheless, a better-chosen parameter b will improve the tracking ability of the system. This figure also shows that the best value of b cannot be found only based on instantaneous displacement or velocity alone. The frequency content of the input must also be considered [22,25].

The frequency response of the quarter car model is depicted in Fig. 15(b). A certain critical frequency ω_C as the crossing point of all lines of various b can be located at the frequency of approximately 17.5 rad/s or 2.79 Hz. For the frequency lower than ω_C, the gain decreases with increasing b. Thus, the greater value of b is better for suppressing lower frequency disturbance. For the frequency higher than ω_C, the gain decreases with decreasing b. In this case, a smaller value of b is preferable to filter high-frequency.

The time and frequency responses of the quarter-car model confirmed that a semi-active suspension control strategy with the damping coefficient b as the control variable needed to accommodate the information about the frequency content of the road surface as the input [19]. The control objective was to reduce the road surface excitation that would reach the car chassis. This means if the road surface contains mainly low frequency, the damping coefficient is to be increased, and vice versa.

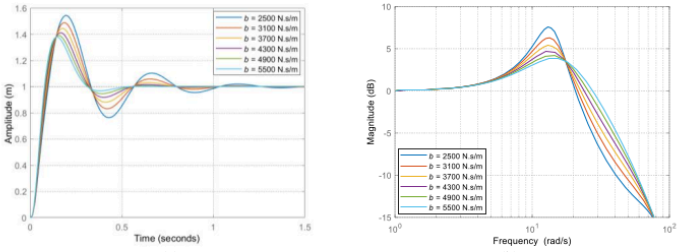

(a) (b)

Fig. 15. The response of the quarter-car model for various damping coefficients; (a) Time response; (b) Frequency response

For illustration, a speed bump in the form of a positive half sinusoidal with an amplitude of 0.1 m and half wavelength of 0.4 m was traveled by the quarter-car model at three different speeds: 3.0 km/h, 6.0 km/h, and 12.0 km/h. The three speeds correspond to the same sinusoidal with the half periods of 0.48 s, 0.24 s, and 0.12 s or the frequency of 1.04 Hz, 2.08 Hz, and 4.17 Hz, respectively. The first two frequencies are below the critical frequency ω_C, while the last is above the critical frequency ω_C.

The response of the quarter-car model to the speed bumps is shown in Fig. 16. In line with the data of system gain in Fig. 15(b), the amplitude of the speed bump (0.1 m) is amplified by the car chassis (to be around 0.13 m) for the first two speeds or frequencies. At the last speed or frequency, with a gain of less than 1, the maximum displacement of the car chassis is less than 0.1 m. Minor changes in the transient responses can also be observed.

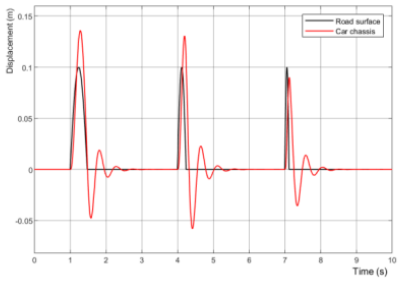

Fig. 16. Response of the quarter-car model to input of a speed bump traveled at different speeds.

4.5. Design of Fuzzy Logic Controller (FLC)

The control scheme using FLC is shown in Fig. 17. The input to the FLC was the main frequency of the road surface and its first derivative (change of frequency), *i.e.*, whether the frequency was increasing or decreasing. The output of the FLC was the current to the MR damper's coil, consisting of a bulk value (current) and an adjusting fine-tuning value (current change).

A frequency detector was placed directly before the inputs. This frequency detector estimated the frequency of the road surface based on the zero crossing and peak-to-peak intervals. The detector used a tap delay unit to record the previous 200 ms data in estimating the frequency.

The current integrator summed up the current change from time to time. This sum was added to the bulk value of the current to ensure that the current to the coil was always set to a reasonable influential value while still allowing small changes due to the actual condition of the road. The calculated current was fed into the MR damper model, which would deliver the amount of damping force to the suspension system [26,27].

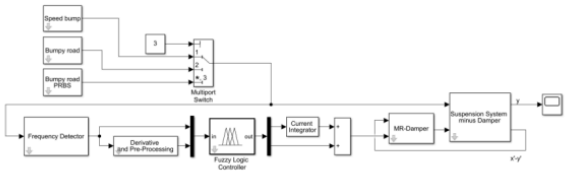

Fig. 17. The proposed control scheme using FLC

A fuzzy rule base consisting of nine rules was constructed and summarized in Table 3. The firing membership functions of the current (I) and the current change (ΔI) were decided based on the road surface's frequency (F) and change of frequency (ΔF).

The fuzzy membership functions for each input are shown in Fig. 18. The frequency range of 0 to 10 Hz was considered adequate to cover the significant frequency of the road surface. The ω_C was placed as the peak of the membership function "Frequency is Middle." Furthermore, the frequency change range was chosen from −1 Hz (decreasing) to +1 Hz (increasing).

Table 3

The fuzzy rule base

I / ΔI		ΔF		
		Neg	*None*	*Pos*
F	*Low*	*High* Increase	*High* Maintain	*High* Decrease
	Middle	*Middle* Increase	*Middle* Maintain	*Middle* Decrease
	High	*Low* Increase	*Low* Maintain	*Low* Decrease

On the output side, the range for current was from 0 to 1,400 mA, the same as the current range used during the experiment. The range for current change was set between −100 mA and +100 mA. The small value was chosen to ensure a gradual change of the current from the bulk current value.

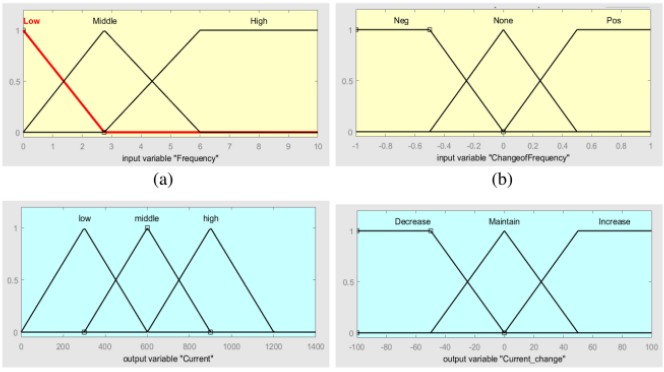

Fig. 18. The fuzzy membership functions (a) Input F; (b) Input ΔF; (c) Output I; (d) Output ΔI

4.6. Test of Control Scheme with Bumpy Road

The bumpy road was modeled to be a road with a sinusoidal contour of amplitude 0.1 m and wavelength of 0.8 m. This road was simulated to be traveled in 3 different speeds: 1.33 m/s (4.8 km/s), 2.67 m/s (9.6 km/h), and 5.33 m/s (19.2 km/h).

The three different speeds are also corresponding to the frequency of 1.67 Hz, 3.33 Hz, and 6.67 Hz. Frequencies were introduced in 1st, 7th, and 13th

seconds. The interval of 6 seconds was set to give the system enough time to reach the new equilibrium.

Fig. 19 shows the comparison between the road surface as the input and the car chassis displacement as the output for both cases of passive suspension system and semi-active suspension system. The oscillation produced by the semi-active (red line) had less amplitude in all cases, with a significant decrease for the second and third frequencies.

Fig. 20(a) shows the detected frequencies of the road surface, which were 1.67 Hz, 3.33 Hz, and 6.67 Hz. The frequency detector was successful in performing the detection within 3 seconds. Fig. 20(b) shows how the current to the MR-damper also decreased gradually according to the increase of the road surface's frequency.

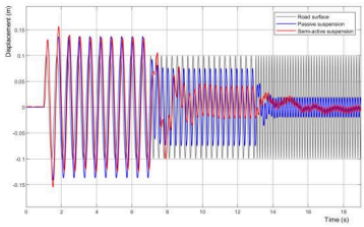

Fig. 19. Comparison between passive and semi-active suspension systems for a bumpy road with three different frequencies (1.67 Hz, 3.33 Hz, and 6.67 Hz).

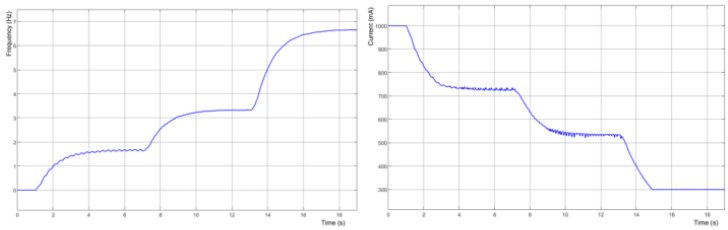

(a) (b)

Fig. 20. The simulation with a bumpy road; (a) The detected frequency; (b) The current trajectory

4.7. Test of Control Scheme with Pseudo-Random Bumpy Road

The pseudo-random bumpy road was the road that consisted of flat segments in the multiplication of 4.0 m length with the heights varying pseudo-randomly between 0, 0.05 m, and 0.10 m. The traveling velocity was 9.6 km/h,

which corresponded to a 1.5 s interval for each segment. This road simulated abrupt road height changes traveled with moderate speed.

The response of the passive and the semi-active suspension system can be seen in Fig. 21. The semi-active suspension system delivered a lower overshoot and a shorter settling time based on visual examination.

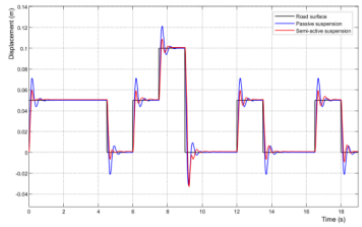

Fig. 21. Comparison between passive and semi-active suspension systems for pseudo-random bumpy road

Fig. 22(a) shows the detected frequency of the road surface. As expected, the detected frequency for a step function was low, with sudden increases during the step changes. Then, this value faded due to the moving average of the measurement data. Fig. 22(b) shows the trajectory of the current supplied to the MR damper, varying around the value of 1,000 mA.

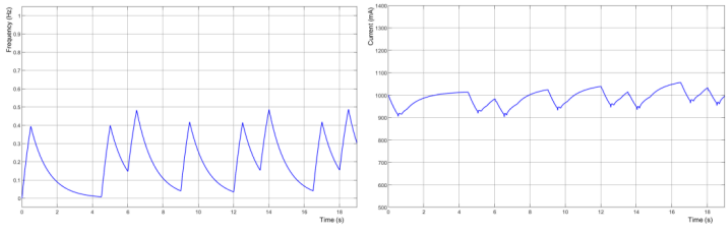

(a) (b)

Fig. 22. The simulation with a pseudo-random bumpy road; (a) The detected frequency; (b) The current trajectory

5. Conclusions

The paper contributes to the development of an implementation-ready semi-active suspension system in two ways: Firstly, inventing a novel modeling approach of a magnetorheological (MR) damper using multiple Artificial Neural Networks (ANNs) and interpolation, and secondly, designing a suitable Artificial

Intelligence (AI) control in the form of a Fuzzy Logic Controller (FLC) for a quarter-car semi-active suspension system using the aforementioned MR damper model.

The proposed MR damper model utilized multiple ANNs to model the relationship between the damping force and the piston velocity for a number of pre-defined coil current values. Interpolation was conducted to determine the damping force for other current values. The MR damper model was tested in the presence of varying current and piston velocity. The test result showed that the model could successfully deliver the best damping force approximates based on the existing experimental data.

The presented FLC method's novelty was that it used the road surface frequency as the input. The control scheme of the semi-active suspension system was tested by using two road surface simulations. The test results showed that the FLC was able to regulate the MR damper so that the semi-active suspension system delivered better performance than the passive suspension system. All time-domain specifications, such as lower amplitude, lower overshoot, and less settling time, were improved.

Acknowledgment

This research is funded by the research grant of the Directorate of Research, Technology, and Community Service, Directorate General of Higher Education, Research, and Technology, Ministry of Education, Culture, Research, and Technology, Indonesia, through the Institute for Research and Community Service of President University, with the contract number 070/LRPM-PFR/VII/PresUniv/2023.

REFERENCES

[1] A.-C. Rădulescu-Gămalet, D. Vasiliu, C. Călinoiu, T. Cojocaru-Greblea, and O. Nica, "Electrohydraulic Braking Systems for Electric and Hybrid Vehicles - Simulations and Experiments," UPB Scientific Bulletin, Series C: Electrical Engineering and Computer Science, vol. 84, iss. 3, pp. 293-308, 2022.

[2] C.-V. Strejoiu, M. G. Osman, and A. C. Cernat, "Towards Sustainable Transportation: Modeling and Simulation of PV Panel Implementation On National Highways for Charging Electric Vehicles Which Leads to Mitigate Carbon Emission," UPB Scientific Bulletin, Series C: Electrical Engineering and Computer Science, vol. 85, iss. 4, pp. 321-334, 2023.

[3] J. S. Núñez and L. E. Muñoz, "Modelling and frequency analysis of semi-active controlled suspension systems of an automobile," Vibroengineering Procedia, vol. 3, pp. 64–69, Oct. 2014.

[4] J. Gołdasz, "Developments in modeling of magnetorheological actuators," Magnetorheological Materials and their Applications, pp. 63–91, 2019. doi:10.1049/pbcs058e_ch4.

[5] Y. Liu, A. Li, Z. Sun, and S. Chen, "Theoretical design and experimental study of magnetic circuit for magnetorheological (MR) damper of shear-valve mode," Advanced Electromagnetics, vol. 11, no. 4, pp. 84–89, 2022. doi:10.7716/aem.v11i4.2055.

[6] H. Li, I. Jönkkäri, E. Sarlin, and F. Chen, "Experimental comparison of constitutive models for magnetorheological fluids under different conditions," Braz. J. Phys., vol. 51, no. 6, pp. 1735–1746, 2021, doi: 10.1007/s13538-021-00989-2.

[7] G. Li and Z.-B. Yang, "Modelling and analysis of a magnetorheological damper with nonmagnetized passages in piston and minor losses," Shock and Vibration, vol. 2020, pp. 1–12, 2020. doi:10.1155/2020/2052140.

[8] R. Zalewski, J. Nachman, M. Shillor, and J. Bajkowski, "Dynamic model for a magnetorheological damper," Applied Mathematical Modelling, vol. 38, no. 9–10, pp. 2366–2376, 2014. doi:10.1016/j.apm.2013.10.050.

[9] Y.-T. Choi and N. M. Wereley, "Nondimensional quasisteady analysis of a magnetorheological dashpot damper," Electrorheological Fluids and Magnetorheological Suspensions (ERMR 2004), 2005. doi:10.1142/9789812702197_0098.

[10] B. Ju, "The simulation and optimization of the magnetic circuit for magnetorheological damper," International Journal of Magnetics and Electromagnetism, vol. 5, no. 1, pp. 1–9, 2019. doi:10.35840/2631-5068/6516.

[11] M. F. Yakhni, M. N. Ali, and M. A. El-Gohary, "Magnetorheological damper voltage control using artificial neural network for optimum vehicle ride comfort," Journal of Mechanical Engineering and Sciences, vol. 15, no. 1, pp. 7648–7661, 2021. doi:10.15282/jmes.15.1.2021.03.0603.

[12] S. Walavalkar, V. Tandel, R. S. Thakur, V. V. P. Kumar, and S. Bhuran, "Performance comparison of various controllers on semi-active vehicle suspension system," ITM Web of Conferences, vol. 40, p. 01001, 2021. doi:10.1051/itmconf/20214001001.

[13] J. de Lozoya-Santos, R. Morales-Menendez, and R. A. Ramírez Mendoza, "Control of an automotive semi-active suspension," Mathematical Problems in Engineering, vol. 2012, pp. 1–21, 2012. doi:10.1155/2012/218106.

[14] T. Ergin and M. Ö. Yatak, "Optimal control method of semi-active suspension system and processor-in-the-loop verification," Applied Sciences, vol. 13, no. 20, p. 11253, Oct. 2023, doi: 10.3390/app132011253.

[15] E. Sitompul, L. Anggraini, A. Sagala, N. Le Hoa, M. Turnip, and A. Turnip, "Enhancing comfort and handling in semi-active suspension systems with fuzzy controller," in Proceedings of the International Conference of Computer Science and Information Technology (ICOSNIKOM), 2023. doi:10.1109/icosnikom60230.2023.10364378.

[16] G. Li and Z.-B. Yang, "Modelling and analysis of a magnetorheological damper with nonmagnetized passages in piston and minor losses," Shock and Vibration, vol. 2020, pp. 1–12, 2020. doi:10.1155/2020/2052140.

[17] D. Q.Truong and K. K. Ahn, "Mr fluid damper and its application to force sensorless damping control system," Smart Actuation and Sensing Systems - Recent Advances and Future Challenges, 2012. doi:10.5772/51391.

[18] Bohai New Materials, "Bohai MR dampers," Series C datasheet, March 2022.

[19] T. A. Arslan, F. E. Aysal, İ. Çelik, H. Bayrakçeken, and T. N. Öztürk, "Quarter car active suspension system control using fuzzy controller," Engineering Perspective, vol. 4, no. 4, pp. 33–39, 2022, doi: 10.29228/eng.pers.66798.

[20] S. Ebrahimi-Nejad, M. Kheybari, and S. V. Borujerd, "Multi-objective optimization of a sports car suspension system using simplified quarter-car models," Mechanics & Industry, vol. 21, no. 4, p. 412, 2020. doi:10.1051/meca/2020039.

[21] J. Hurel, J. Amaya, J. Peralta, D. Alvarado, and F. Flores, "Particle Swarm Optimization Applied on Fuzzy Control: Comparative analysis for a Quarter-car Active Suspension

Model," 2022 IEEE International Conference on Industrial Technology (ICIT), Shanghai, China, 2022, pp. 1-8, doi: 10.1109/ICIT48603.2022.10002809.

[22] E. Sitompul and M. Y. Baihaqi, M.Y, "Quasi-dynamic walking optimization of humanoid robot using genetic algorithm," International Journal of Artificial Intelligence, vol. 20, no. 1, pp. 24–45, 2022.

[23] A. Iantoc, C. Bulac, and D. Sidea, "Optimal Reactive Power Dispatch in Active Distribution Power Systems Using Grey Wolf Optimizer," UPB Scientific Bulletin, Series C: Electrical Engineering and Computer Science, vol. 84, iss. 3, pp. 235-246, 2022.

[24] M. Saad, S. Akhtar, A. K. Rathore, Q. Begume, and M. Reyaz-ur-Rahim, "Control of semi-active suspension system using PID Controller," IOP Conference Series: Materials Science and Engineering, vol. 404, p. 012039, 2018. doi:10.1088/1757-899x/404/1/012039.

[25] P. Turnip, E. Sitompul, B. M. Wibawa, A. Trisanto, and A. Turnip, "Motor speed control toward wall surface angle based on HC-SR04 ultrasonic sensor," in Proceedings of the International Conference on Culture Heritage, Education, Sustainable Tourism, and Innovation Technologies, SCITEPRESS - Science and Technology Publications, 2020.

[26] Z. Li and H. Dai, "Vehicle semi-active suspension system simulation with Variable Structure Control Method," ICCTP, 2009. doi:10.1061/41064(358)472.

[27] Y. M. Al-Rawashdeh, S. E. Ferik, and M. A. Abido, "Robust full-car active suspension system," 2019 10th International Conference on Information and Communication Systems (ICICS), 2019. doi:10.1109/iacs.2019.8809167.

Turnitin_Lidya10

ORIGINALITY REPORT

9%	6%	7%	3%
SIMILARITY INDEX	INTERNET SOURCES	PUBLICATIONS	STUDENT PAPERS

PRIMARY SOURCES

1	president.ac.id Internet Source	2%
2	repository.president.ac.id Internet Source	1%
3	Hemanth, K., A. Ganesha, Kumar Hemantha, and K.V. Gangadharan. "Analysis of MR Damper Based on Finite Element Approach", Applied Mechanics and Materials, 2014. Publication	1%
4	Jung Woo Sohn, Jong-Seok Oh, Seung-Bok Choi. "Design and novel type of a magnetorheological damper featuring piston bypass hole", Smart Materials and Structures, 2015 Publication	1%
5	Abdelmoneam Elsaady, Wael M. A.. "Time-Dependent Computational Fluid Dynamics and Quasi-Static Analysis of Smart Dampers", The University of Manchester (United Kingdom), 2025 Publication	1%
6	www.mdpi.com Internet Source	1%
7	S.C. Lim. "Design and analysis programme of electrorheological devices for vehicle	1%

systems", International Journal of Vehicle Autonomous Systems, 2005
Publication

8 Martin Rosenberger, Manfred Pl[?]chl, Klaus Six, Johannes Edelmann. "The Dynamics of Vehicles on Roads and Tracks - Proceedings of the 24th Symposium of the International Association for Vehicle System Dynamics (IAVSD 2015), Graz, Austria, 17-21 August 2015", CRC Press, 2019 — 1 %
Publication

9 S. H. Yahaya, S. F. Yaakub, F. Ahmad, M. S. Salleh, M. Y. Yuhazri, S. Akmal. "Comparison study for double passive car suspension system through mathematical modelling and experimental work", International Journal of Advanced Technology and Engineering Exploration, 2021 — 1 %
Publication

10 Lydia Anggraini, Ventika Aurora Pratiwi. "Machine Tonnage Optimization by Reused Scrap Material Applied for Car Propeller Shaft Guard", 2019 International Conference on Sustainable Engineering and Creative Computing (ICSECC), 2019 — 1 %
Publication

11 unis.yalova.edu.tr — 1 %
Internet Source

Exclude quotes	On	Exclude matches	< 1%
Exclude bibliography	On		

Turnitin_Lidya10

GRADEMARK REPORT

FINAL GRADE

/0

GENERAL COMMENTS

PAGE 1

PAGE 2

PAGE 3

PAGE 4

PAGE 5

PAGE 6

PAGE 7

PAGE 8

PAGE 9

PAGE 10

PAGE 11

PAGE 12

PAGE 13

PAGE 14

PAGE 15

PAGE 16

PAGE 17

PAGE 18

PAGE 19

PAGE 20